Femtosecond wavepacket dynamics of Cs adsorbates on Pt(111): Coverage and temperature dependences

Kazuya Watanabe, Noriaki Takagi, and Yoshiyasu Matsumoto*
Department of Photoscience, The Graduate University for Advanced Studies (Sokendai), Hayama, Kanagawa 240-0193, Japan and Institute for Molecular Science, Okazaki, Aichi 444-8585, Japan
(Received 18 June 2004; revised manuscript received 24 November 2004; published 17 February 2005)

Femtosecond time-resolved second harmonic generation (TRSHG) has been used to observe vibrational wavepacket dynamics at a Cs-covered Pt(111) surface. The creation and dephasing of vibrational coherence are monitored via the intensity modulations in the second harmonic of probe pulses as a function of pump-probe delay. The oscillatory signals are found in TRSHG signals upon the excitations at 580 and 800 nm, which are the manifestation of nuclear wavepacket dynamics on the surface. The Cs-coverage dependence studied in detail indicates that the wavepacket dynamics of Cs-Pt stretching modes and Pt surface phonon modes are responsible for the TRSHG signals. The cos-like initial phase of the oscillatory signals and the coverage dependence of the initial amplitude suggest that the vibrational coherence is associated with the resonant excitation between Cs-derived states in the quantum well of the Cs overlayer. The rate of Cs-Pt vibrational dephasing increases with the surface temperature. This behavior cannot be accounted for by the increasing contribution from the hot bands of the Cs-Pt stretching mode. Instead, pure dephasing caused by anharmonic coupling between Cs-Pt stretching and parallel modes in the Cs overlayer is likely the dominant mechanism for the vibrational dephasing.

DOI: 10.1103/PhysRevB.71.085414 PACS number(s): 78.47.+p, 68.43.Pq, 68.35.Ja, 82.53.St

I. INTRODUCTION

The control of molecular dynamics by tailored ultrashort laser pulses demands detailed information on the creation of a nuclear wavepacket and its time evolution. In spite of the growing knowledge on the nuclear wavepacket dynamics in gases and in bulk solids, the wavepacket dynamics of adsorbates on solid surfaces has been scarcely studied. Recently, time-resolved second harmonic generation (TRSHG) has been demonstrated to be a powerful tool to investigate the dynamics of vibrational coherence at solid surfaces.[1–3] We have applied this technique to cesium atoms adsorbed on Pt(111) to observe the vibrational coherence of the Cs---Pt stretching mode in the time domain.[4,5] In our previous paper,[5] we have focused on the dephasing dynamics of the Cs-Pt stretching mode under the influence of substrate hot electrons induced by laser irradiation. As the pump laser fluence increases, the dephasing rate significantly increases. The enhancement of dephasing at high pump fluences is accounted for by elastic and/or inelastic scatterings of hot electrons at Cs on the surface.

To understand the excitation mechanism for the vibrational coherence at the surface and subsequent dephasing dynamics, we need more precise information on the behavior of TRSHG signals. In this paper, we describe the Cs-coverage θ dependence of TRSHG signals obtained from Cs/Pt(111) by using two different femtosecond light sources: the central frequency of 800 nm with the duration of 130 fs, and 580 nm with the duration of 25 fs. In our previous reports,[4,5] the measurements were performed at $\theta \sim 0.27$ ML, where the TRSHG signals representing Cs—Pt dephasing dynamics are well fitted by a single exponentially damped oscillating function as long as pump fluence is moderate. However, in this paper, we show that TRSHG signals drastically changes their waveforms as θ is varied. Oscillatory signals are observed only in $\theta > 0.2$ ML and their features depend on the photon energy of the employed light source. Analysis by linear prediction singular value decomposition (LPSVD) indicates that not only the Cs-Pt stretching mode, but Pt surface phonon modes (Rayleigh modes) contribute to the signals. We discuss the excitation mechanism for the vibrational coherence based on coverage and wavelength dependences. We also examine the surface-temperature dependence of TRSHG signals, which provides a clue for the origin of dephasing in the Cs-Pt vibrational coherence.

II. EXPERIMENT

The experiments were carried out in an ultrahigh vacuum (UHV) chamber equipped with a cylindrical mirror analyzer for Auger electron spectroscopy.[4] Cs atoms from a well-degassed alkali dispenser (SAES getters) were deposited on a clean Pt(111) surface at 110 K. Cs coverages were determined by Auger electron spectroscopy and work function measurements. The procedure for TRSHG measurements is basically the same as previously reported.[4] Briefly, near-infrared (800 nm) laser pulses with the duration of 130 fs from a Ti:sapphire regenerative amplifier (Spectra Physics, Spitfire, 1 kHz) were separated into two beams for pump and probe pulses. Both of the *p*-polarized beams were focused on the sample surface in the UHV chamber. Second harmonic (SH) signals in *p*-polarization were generated by the probe beam coaxially, passed through a band pass filter, and were detected by a photomultiplier tube. A chopper was inserted in the optical path of the pump beam for the lock-in detection of pump-induced SH intensity modulations as a function of the pump-probe delay t. The spatial and temporal overlaps of the two beams were confirmed by monitoring the sum frequency signals of pump and probe pulses from the sample surface.

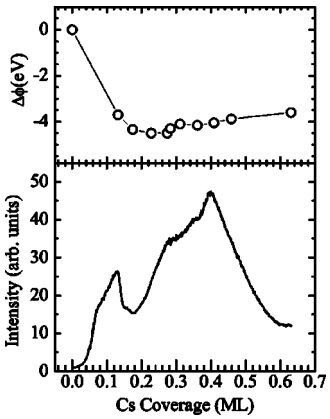

FIG. 1. Variations in SH intensity (solid curve) and work function changes $\Delta\phi$ (circles) as a function of Cs coverage. The wavelength of the excitation laser is 800 nm.

A home-built noncollinear optical parametric amplifier (NOPA) was also used as the other light source.[6] The NOPA system was modified to supply two independent outputs by splitting an OPA pump beam (400 nm) into two for pumping two β-barium borate (BBO) crystals. This provides us two ultrashort pulse sources tunable from 490 to 720 nm. In this work, the wavelengths of both of the NOPA outputs were fixed at 580 nm and used for pump and probe beams. For the measurements with the NOPA light source, a 1 mm thick fused silica plate was used as a laser inlet of the UHV chamber for reducing pulse broadening by dispersion through the optics. The NOPA output energy was $\sim 4\ \mu$J/pulse right after the BBO crystal and the fluence absorbed at the sample surface was estimated to be $\sim 500\ \mu\text{J/cm}^2$. From the cross correlation profile of pump and probe pulses at the sample surface, the pulse duration was estimated to be 25 fs. Hereafter, measurements with the Ti:sapphire fundamental light are denoted as 800-nm pump, while those with NOPA are denoted as 580-nm pump.

Throughout this paper, the transient change of SH intensity $\Delta\text{SH}(t)$ is defined as $\Delta\text{SH}(t)=(\text{SH}(t)-\text{SH}^{\circ})/\text{SH}^{\circ}$, where $\text{SH}(t)$ and SH° are the SH intensities with and without pump pulses, respectively. The sample temperature was kept at 110 K during the measurements, if not specified.

III. RESULTS AND DISCUSSION

A. SH intensity vs Cs coverage

The lower panel of Fig. 1 shows the intensity variation in SH° of 800-nm pulses while Cs was continuously deposited onto a clean Pt(111) surface. The changes in work function are also plotted in the upper panel. The work function decreases steeply in the beginning of Cs deposition and reaches a minimum at $\theta\sim 0.25$ ML ($1\ \text{ML}=1.5\times 10^{15}\ \text{cm}^{-2}$). The SH intensity is remarkably enhanced with the Cs deposition and shows strong maxima at $\theta\sim 0.12$ and ~ 0.4 ML. The strong enhancement in SHG induced by an alkali-metal overlayer has been commonly observed in the systems of alkali-metal overlayers on metals. The origins of the enhancement are attributed to the local-field enhancement at an adsorbate-vacuum interface and/or interband transitions between two-dimensional alkali-metal adsorbate induced states.[7–12]

The prominent peak at $\theta\sim 0.12$ ML in Fig. 1 can be due to a two-photon resonance transition between Cs-induced occupied and unoccupied states as in the case of Cs on Cu(111) observed by Lindgren and Walldén.[9] On the other hand, a weak hump at $\theta\sim 0.28$ ML is likely due to a one-photon resonance transition between the Cs-induced states, since the vacuum level is lowered to ~ 1.5 eV above the Fermi level at this coverage. In $\theta > 0.28$ ML, the SH intensity increases with θ owing to the local-field enhancement at the adsorbate-vacuum interface and/or the interband transitions between the Cs-induced states. The Cs overlayer becomes metallic in this coverage range.[13] Thus, the Cs-induced states involved in the SH enhancement are the ones in a quantum well (QW) confined within the Cs layer as reported for Na/Cu(111).[14] In $\theta > 0.4$ ML, the SH intensity decreases rapidly, indicating that the photon energy deviates from the exact resonance of the interband transition.

B. The origin of TRSHG signals

Several factors influence ΔSH, including electron dynamics in the bulk and Cs overlayer, and coherent nuclear wavepacket dynamics at the surface. Under a crude approximation, the effective second order susceptibility for SH generation at the Cs/Pt(111) surface $\chi^{(2)}_{\text{eff}}$ can be decomposed into a Cs-derived component $\chi^{(2)}_{\text{Cs}}$ and a substrate component $\chi^{(2)}_{\text{Pt}}$. The photoinduced modulations of these terms can be expressed in terms of the transient electronic temperature of Pt substrate T_e, the population change in a Cs-derived electronic band δn_k and the nuclear displacement along a vibrational mode δQ_i, where k and i are the indices for Cs-derived electronic bands and vibrational (phonon) modes, respectively. If δQ_i and δn_k are small, $\chi^{(2)}_{\text{eff}}$ can be expanded in terms of these terms. When we truncate the expansion at the first order, $\chi^{(2)}_{\text{eff}}$ is written as

$$\chi^{(2)}_{\text{eff}} = \chi^{(2)}_{\text{Cs}}|_0 + \sum_i \left.\frac{\partial\chi^{(2)}_{\text{Cs}}}{\partial Q_i}\right|_0 \delta Q_i + \sum_k \left.\frac{\partial\chi^{(2)}_{\text{Cs}}}{\partial n_k}\right|_0 \delta n_k + \chi^{(2)}_{\text{Pt}}|_0 + \delta\chi^{(2)}_{\text{Pt}}(T_e). \quad (1)$$

Here, $\chi^{(2)}_{\text{Cs}}|_0$ and $\chi^{(2)}_{\text{Pt}}|_0$ denote the pump-independent parts of $\chi^{(2)}_{\text{eff}}$. The second and third terms are due to the variations of $\chi^{(2)}_{\text{Cs}}$ by nuclear displacements and by electronic population changes in Cs-derived states, respectively. The last term represents the variation of $\chi^{(2)}_{\text{Pt}}$ by the changes in electronic temperature of Pt substrate. Since SH intensity is proportional to the square of $\chi^{(2)}_{\text{eff}}$, ΔSH is mainly determined by the following terms:

$$\Delta\text{SH} \propto \sum_i \chi^{(2)}_{\text{Cs}}|_0 \cdot \left.\frac{\partial\chi^{(2)}_{\text{Cs}}}{\partial Q_i}\right|_0 \delta Q_i + \sum_k \chi^{(2)}_{\text{Cs}}|_0 \cdot \left.\frac{\partial\chi^{(2)}_{\text{Cs}}}{\partial n_k}\right|_0 \delta n_k + (\chi^{(2)}_{\text{Cs}}|_0 + \chi^{(2)}_{\text{Pt}}|_0)\cdot\delta\chi^{(2)}_{\text{Pt}}(T_e), \quad (2)$$

where all the smaller second order terms are neglected. Equation (2) indicates that SH modulations caused by nuclear wavepacket motion are linear to its displacement.

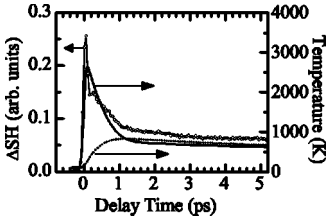

FIG. 2. A typical TRSHG trace (open circle) obtained from a clean Pt(111) surface. The fluence of the 800-nm pump pulse absorbed was 4.5 mJ/cm^2. Shown together are the calculated profiles of electron (solid curve) and lattice (dashed curve) temperatures. The initial temperature was set to be 110 K. The calculations were performed for a Gaussian pulse with the duration of 130 fs and the absorbed fluence of 4.5 mJ/cm^2.

C. The coverage dependence of oscillatory signals

TRSHG signals generated from a clean Pt(111) surface is plotted in Fig. 2. At the clean surface, the signals show fast and slow decaying components. The decaying signals in $t > 250$ fs are well fitted by a double-exponential function with time constants of 410 fs and 2.76 ps. No oscillatory signals are detected from the clean surface. Figure 2 also shows the temporal variations in electronic and lattice temperatures (T_e and T_{lat}, respectively) at the Pt(111) surface, estimated by the numerical integration of coupled diffusion equations with the thermodynamic coefficients of bulk Pt.[15] Since the temporal profile of $\Delta\mathrm{SH}(t)$ is similar to that of T_e, the signals originate mainly from hot electrons generated by the transient heating of the Pt substrate, i.e., $\chi^{(2)}_{\mathrm{Pt}}|_0 \cdot \delta\chi^{(2)}_{\mathrm{Pt}}(T_e)$.

Figure 3 shows the coverage dependence of TRSHG signals from Cs/Pt(111) generated by 800-nm pump. At $\theta = 0.12$ ML, although the ΔSH signals deflect in the direction opposite to that of the clean surface, the overall temporal profile of the TRSHG signals is similar to that obtained from the clean surface. From Eq. (2), the reversed deflection of ΔSH at $\theta = 0.12$ ML is understood, provided that $\chi^{(2)}_{\mathrm{Cs}}|_0$ and $\chi^{(2)}_{\mathrm{Pt}}|_0$ possess an opposite sign to each other and $|\chi^{(2)}_{\mathrm{Cs}}|_0| \gg |\chi^{(2)}_{\mathrm{Pt}}|_0|$. Thus, the TRSHG signals at $\theta = 0.12$ ML also reflect the transient changes in T_e. Since the Cs-derived terms grow with θ, the contribution of substrate heating $\delta\chi^{(2)}_{\mathrm{Pt}}(T_e)$ to the signals becomes relatively small.

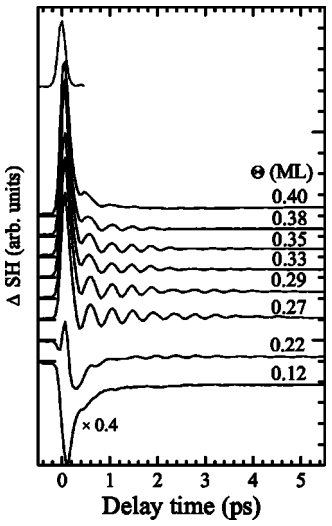

FIG. 3. Cs-coverage dependence of TRSHG signals for 800 -nm pump. The pump fluence was 4.5 mJ/cm^2 for 0.12 ML and 1.8 mJ/cm^2 for the others. The top trace shows a cross correlation of pump and probe pulses. Zero in intensity for each trace is indicated by a solid bar on the left-hand side.

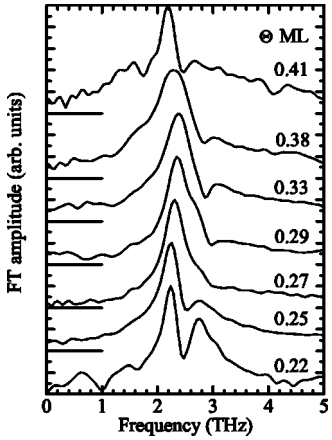

FIG. 4. Fourier amplitude spectra of the oscillatory parts of TRSHG signals for 800-nm pump at various Cs coverages. The spectra are normalized at their peaks.

Upon further increase in θ, oscillatory signals were clearly observed. For $\theta > 0.22$ ML, a strong peak at $t \sim 0$ ps appears in each spectrum. This peak may be due to the ultrafast dynamics of electrons in Cs-derived unoccupied states (see below). Since the laser pulse width is not short enough to distinguish the contributions of nuclear dynamics from those of electron dynamics, it is difficult to analyze the oscillatory signals unambiguously. Thus, we focus on the signals at $t > 250$ fs for 800-nm pump, where the contributions of electron dynamics are negligible.

Figure 4 shows the Fourier transform (FT) spectra of the oscillatory parts in the TRSHG signals for 800-nm pump at various Cs coverages. We deduced the oscillatory parts from the raw data in $t > 250$ fs by subtracting background components whose frequencies are less than 1 THz. Each FT spectrum in Fig. 4 shows a main peak at 2.2–2.4 THz, whose frequency varies with θ. Since the frequencies are close to those of the Cs stretching modes on Ru(0001) ($\sim$2.1 THz at 0.2 ML) (Ref. 16) and Cu(001) ($\sim$1.6 THz at 0.27 ML),[17] the main peak is attributed to the Cs—Pt stretching mode. Note that there is a clear dip at 2.5 THz in the spectrum at $\theta = 0.22$ ML. The dip frequency and its depth change with θ. The appearance of the dip indicates that some other components coexist near the frequency of the Cs-stretching mode.

Figure 5 shows the detailed coverage dependence of TRSHG signals obtained by 580-nm pump. Although the spectral features are similar to those in Fig. 3, some distinctions are apparent. Each spectrum taken with $\theta \geqslant 0.26$ ML shows a relatively strong peak at $t \sim 200$ fs, as in the case of 800-nm pump. However, in contrast to Fig. 3, the peak is well separated in the time domain from the pump pulse thanks to the much shorter pulse duration in 580-nm pump

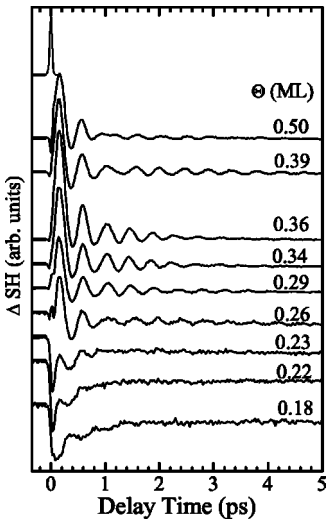

FIG. 5. Cs-coverage dependence of TRSHG signals for 580 -nm pump. The top trace shows a cross correlation trace of pump and probe pulses. The pump fluence was 0.5 mJ/cm^2.

than 800-nm pump. Thus, this is not caused by coherent artifact discussed before,[5] but rather reflects nuclear wavepacket dynamics.

Figure 6 shows the FT spectra of the oscillatory parts in TRSHG signals for 580-nm pump. These spectra were obtained by the similar procedure as in Fig. 4 except for using the time-domain data in $t>50$ fs. A strong peak in 2.2–2.4 THz is due to the Cs-Pt stretching mode. Each spectrum taken in $0.22<\theta<0.26$ ML and $\theta>0.39$ ML shows a dip at ~2.5 THz and an additional peak in 2.6–2.8 THz. In the spectra of $0.34<\theta<0.36$ ML, a dip at ~2.9 THz is apparent, as in Fig. 4.

When a molecular system is resonantly excited, vibrational wavepacket dynamics can be observed both on the potential energy surfaces of ground and electronically excited states.[18] In this case, the ground-state wavepacket is induced by "resonant impulsive Raman scattering" and expressed as the depletion of initial ground state population

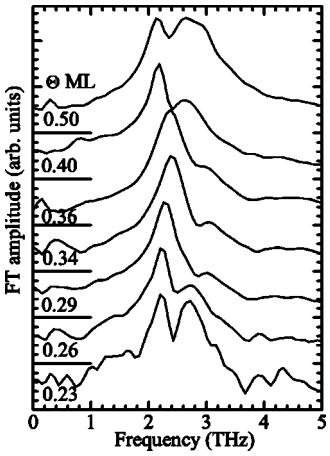

FIG. 6. Fourier amplitude spectra of the oscillatory parts of TRSHG signals for 580-nm pump at various Cs coverages. The spectra are normalized at their peaks.

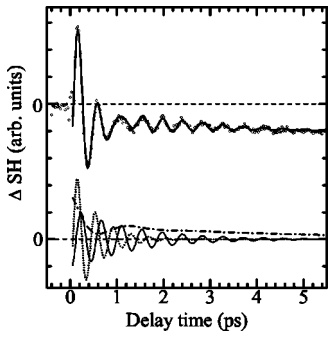

FIG. 7. Fitting results (upper trace) and the LPSVD analysis (lower traces) of the data at $\theta=0.26$ ML by 580-nm pump. Open circles in the upper trace: the experimental data. Thin solid curve, 2.30 THz damped cosine. Dots, 2.61 THz damped cosine. Dashed-dotted curve, the summation of the components of $(\omega/2\pi,\tau)$ = (0 THz, 4.29 ps) and (0.72 THz, 0.47 ps). Thick solid curve (top), a linear combination of the components plotted below. See Table I for the details of parameters.

(hole).[19,20] Vibrational wavepacket dynamics in both excited and ground states were reported first on molecular systems and later on the F centers in KBr[21] and halogen-bridged mixed valence linear chain complexes.[22,23]

As for Cs/Pt(111), the Cs adlayers showing the oscillatory signals likely form 2D confined QW states. Thus, the resonant excitation of inter-QW states by an ultrashort pulse may generate wavepackets both in the ground and excited states in 2D quantum well. However, the oscillatory signals in Figs. 3 and 5 are not likely due to the wavepacket motion in the excited state, since the dephasing time longer than 1 ps is too long compared with the excited state lifetime of the adsorbate.[24] Thus, the main peak at 2.2–2.4 THz is due to the wavepacket dynamics of the Cs—Pt stretching modes in the ground state.

D. LPSVD analysis

To obtain a deeper insight into the time evolution of wavepacket dynamics, the time domain data were fit to a sum of exponentials and exponentially damped cosinusoids by using the linear prediction singular value decomposition (LPSVD) based on the procedure described in Refs. 25 and 26. The following functional form of TRSHG signals is assumed in the analysis,

$$\Delta \mathrm{SH} = \sum_i A_i \cos(\omega_i t + \phi_i)\exp(-t/\tau_i). \tag{3}$$

In the analysis, the TRSHG signals in $t>50$ fs ($t>0.25$ ps) are used for 580-nm (800-nm) pump, and a constant background is subtracted from each trace prior to the analysis. The typical fitting results and the LPSVD analysis are shown in Figs. 7 and 8 for $\theta=0.26$ and 0.40 ML, respectively. The LPSVD fittings give 4–5 components whose frequencies range from 0–3 THz. The obtained parameters are plotted in Fig. 9 and summarized in Tables I and II. Typical errors are ±2% for frequency, ±10% for dephasing time, and ±14° for initial phase. These were estimated by the statistical distributions of the fitted parameters obtained in the different sets of data.

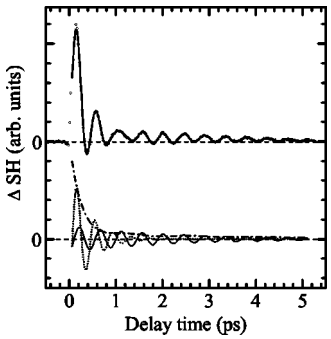

FIG. 8. Fitting results (upper trace) and the LPSVD analysis (lower traces) of the data at $\theta=0.40$ ML by 580-nm pump. Open circles in the upper trace, the experimental data. Thin solid curve, 2.23-THz damped cosine. Dots, 2.56-THz damped cosine. Dashed-dotted curve, the summation of the exponentially decaying components of $\tau=3.84$ and 0.23 ps, the 0.74-THz damped cosine function. See Table I for the details of parameters.

The components obtained from the fittings are classified in two types: one is a damped cosinusoid with $\omega/2\pi > 2$ THz and the other below 1 THz. The former originates from the vibrational wavepacket motions, and the latter from merely electronic responses. In $\theta > 0.25$ ML, the low frequency components with $\tau=200-300$ fs contribute largely, irrespective of the pump wavelength. These rapidly decaying background components may be ascribed to the ultrafast decay dynamics of electrons excited into a Cs-induced unoccupied QW state, and are likely responsible for the strong peak observed at $t\sim 0$ in the time-domain data for 800-nm pump.

As described earlier, the damped cosinusoids with $\omega/2\pi = 2.2-2.4$ THz are due to the wavepacket motion of the Cs-Pt stretching mode. In addition, there are other components contributing to the TRSHG traces, 2.5–2.6 THz in $0.23 \leqslant \theta \leqslant 0.29$ ML and ~2.9 THz in $0.29 \leqslant \theta \leqslant 0.36$ ML. In the following, we discuss the possible origins for these components.

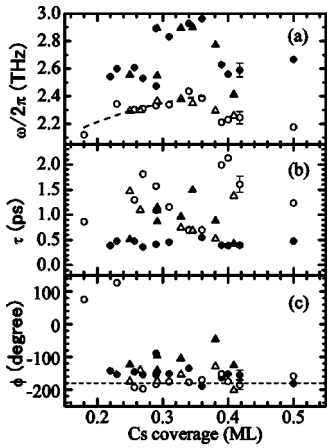

FIG. 9. LPSVD fitting parameters as a function of Cs coverage, (a) frequency, (b) dephasing time, and (c) initial phase. Open circles and open triangles are for Cs-Pt stretching modes for 580-nm pump and 800-nm pump, respectively. Filled circles and filled triangles are for additional components with frequencies higher than 2.45 THz for 580-nm pump and 800-nm pump, respectively. Typical errors are ±2% for frequency, ±10% for dephasing time, and ±14° for initial phase. The dashed curve in (a) shows a fitting result by Eq. (4). The dashed horizontal line in (c) indicates $\phi=-180°$, i.e., cos dependence.

TABLE I. Parameters obtained from the LPSVD analysis of TRSHG signals for 580-nm pump.

θ (ML)	$\omega/2\pi$ (THz)	τ (ps)	ϕ (deg)	A
0.23	2.60	0.48	−153	0.28
	2.34	4.73	127	0.03
	0	1.33	0	0.15
	0	0.39	0	−0.54
0.26	2.61	0.48	−145	0.51
	2.30	1.30	−193	0.20
	0.72	0.47	2	0.18
	0	4.29	0	0.10
0.27	2.31	1.81	−197	0.11
	2.53	0.36	−154	0.49
	0	9.92	0	0.07
	0	0.22	0	0.33
0.29	2.89	1.09	−88	0.06
	2.47	0.42	−155	0.46
	2.33	1.57	−183	0.12
	0.76	0.32	−25	0.25
	0	0.91	0	0.11
0.34	2.92	0.71	−135	0.10
	2.44	0.69	−177	0.39
	0.73	0.33	−8	0.32
	0.43	3.51	−34	0.01
	0	0.76	0	0.18
0.36	2.96	0.55	−189	0.10
	2.39	0.70	−170	0.31
	0	2.59	0	0.04
	0	0.21	0	0.55
0.40	2.56	0.39	−152	0.42
	2.23	2.13	−175	0.08
	0.74	1.62	−18	0.01
	0	3.84	0	0.04
	0	0.23	0	0.45

In these coverage regions, it is known that alkali-metal overlayer forms a couple of superstructures, (2×2) at $\theta=0.25$ ML and $(\sqrt{3}\times\sqrt{3})R30°$ at $\theta=0.33$ ML.[27,28] In $\theta > 0.33$ ML, $(\sqrt{3}\times\sqrt{3})$ domains are mixed with incommensurate hexagonal domains and at $\theta=0.41$ ML, the first layer of Cs is completed and the incommensurate hexagonal domains are formed with rotational disorder.[27]

In the (2×2) domain, the phonon mode at $\bar{M}$ of the clean surface is folded to $\bar{\Gamma}$, so that the phonon mode at the zone boundary becomes optically active. The frequency of the surface Rayleigh phonon mode at $\bar{M}$ on Pt(111) was reported to be 10.8 meV (2.6 THz),[29] which is very close to that of the

TABLE II. Parameters obtained from the LPSVD analysis of TRSHG signals for 800-nm pump.

θ (ML)	$\omega/2\pi$ (THz)	τ (ps)	ϕ (deg)	A
0.22	2.68	0.88	−142	0.09
	2.26	1.86	−138	0.06
	1.08	0.53	14	0.08
	0	0.36	0	−0.78
0.25	2.56	0.51	−123	0.26
	2.29	1.47	−174	0.18
	0.09	1.21	−123	0.20
	0	0.18	0	0.36
0.27	2.30	1.09	−140	0.36
	0	4.95	0	0.14
	0	0.70	0	−0.19
	0	0.24	0	0.31
0.29	2.89	1.09	−97	0.07
	2.55	0.87	−141	0.13
	2.36	1.14	−174	0.30
	0.12	4.31	−130	0.03
	0	0.24	0	0.46
0.33	2.89	0.96	−105	0.07
	2.38	0.74	−154	0.30
	0.52	1.44	35	0.02
	0	2.17	0	0.02
	0	0.24	0	0.59
0.38	2.77	0.88	−46	0.04
	2.29	0.52	−129	0.26
	0.29	4.12	−117	0.01
	0	0.20	0	0.69
0.41	2.41	0.43	−125	0.30
	2.26	1.38	−201	0.14
	1.61	1.26	−31	0.04
	0.94	3.20	−220	0.02
	0.13	1.24	18	0.49

additional component found in $0.23 \leqslant \theta \leqslant 0.29$ ML. Thus, the additional component is attributed to the Rayleigh mode at $\bar{M}$ on Pt(111) folded to $\bar{\Gamma}$. On the other hand, the frequency of the surface Rayleigh modes at $\bar{K}$ on a clean Pt(111) surface is reported to be 11.1 meV (2.7 THz),[29] which is comparable to that of the additional component in $0.29 \leqslant \theta \leqslant 0.36$ ML. Thus, by the same token, it is ascribed to the Rayleigh mode at $\bar{K}$ on Pt(111) folded to $\bar{\Gamma}$ because of the Cs-$(\sqrt{3}\times\sqrt{3})$ superstructure.

In $\theta \geqslant 0.39$ ML, the additional component becomes prominent and its frequency decreases, 2.41 THz for 800-nm pump and 2.56 THz for 580-nm pump. In the previous report,[5] we showed that a fast decaying component appears as the pump fluence increases. This component is attributed to the dephasing by substrate hot electron scattering. However, the relative amplitude of this component did not change when the pump fluence was reduced to one-fourth of that employed in Fig. 8. Thus, this component is not caused by the substrate hot electron scattering. A possible origin of the additional component is a Rayleigh phonon mode optically activated by the incommensurate Cs overlayer or a Cs-Pt stretching mode at the domain boundaries. In any case, it is difficult to explain why the relative amplitude of the component is so large, i.e., ~5 times larger than the Cs—Pt stretching mode with $\omega/2\pi = 2.23$ THz.

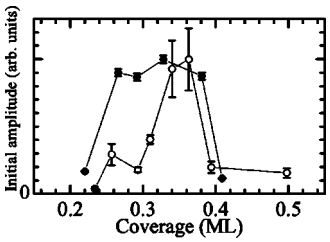

FIG. 10. Variations of an initial amplitude of the Cs-Pt stretching mode as a function of θ. Filled circles, 800-nm pump. Open circles, 580-nm pump.

Note that the LPSVD result at $\theta = 0.40$ (Fig. 8) indicates that the background component with $\tau \sim 400$ fs has a large amplitude. If this background component were due to substrate transient heating, this should match to the TRSHG signal at the clean surface. Although similar decay time components exist on the clean surface (Fig. 2), the substrate transient heating cause relatively large constant background that is absent in Fig. 8. Therefore, this background component is not likely due to the substrate transient heating, but reflect the decay dynamics of photoexcited electrons in the Cs-derived QW states above the Fermi level. It is noteworthy that the dephasing time of the 2.56-THz component (580-nm pump) is close to those of the background component. This indicates that the 2.56-THz component correlates with the electronic decay in the Cs-derived unoccupied states. Thus, another possible origin of this component could be the nuclear wavepacket dynamics of the Cs—Pt mode in the electronically excited states of the Cs-derived QW.

E. Oscillation amplitude vs coverage

The initial amplitude of the Cs—Pt stretching mode with $\omega/2\pi = 2.2-2.4$ THz are plotted in Fig. 10 as a function of θ. Errors were estimated by the statistical distributions of the obtained parameters divided by total SHG intensity and were mainly due to the long-term variation of the laser intensity, in particular, of the NOPA output. In the case of 580-nm pump, the amplitude of the Cs—Pt stretching mode has a peak at $\theta \sim 0.36$ ML. This is consistent with the picture that the creation of vibrational coherence is enhanced by resonant excitation between the Cs derived electronic states. In the case of 800-nm pump, the amplitude has a broad maximum in $0.26 < \theta < 0.38$ ML and decreases at $\theta > 0.4$ ML. This indicates that the pump photon energy (1.55 eV) is close but does not reach to the exact resonance below $\theta = 0.4$ ML and deviate from it owing to a sudden change in the electronic state with the formation of the Cs incommensurate layer.

F. Phase shift vs coverage

The initial phase of oscillatory signals depends on the excitation mechanism of vibrational coherence. The initial

phase for the Cs—Pt stretching mode falls in the range of $-180\pm10°$ in $0.25<\theta<0.5$ ML for 580-nm pump [Fig. 9(c)]. According to the theoretical analysis on impulsive Raman processes,[20,30] the initial phase of vibrational coherence varies as a function of the difference in energy between an excitation photon and a relevant electronic transition. While oscillatory signals show cos-like behavior at exact resonance, the initial phase changes as the excitation photon energy is detuned and finally they show sin-like behavior at complete off-resonance. The Cs—Pt stretching mode exhibits cos-like behavior rather than sin-like, which is consistent with the resonance enhanced impulsive Raman excitation mechanism.

In the case of 800-nm pump for $0.25<\theta<0.38$ ML, the initial phases of the Cs—Pt stretching mode fall in $-150\pm20°$. This is close to cos-like behavior. However, the initial phase changes rather erratically with θ in contrast to 580-nm pump. This is because the pulse width in 800-nm pump (130 fs) is substantially longer than 580-nm pump, which is 1/3 of the vibrational period (~420 fs), so that large errors are unavoidable in the estimations of phases.

G. Frequency shift of the Cs—Pt mode vs coverage

As shown in Fig. 9(a), the peak frequency of the Cs—Pt stretching mode increases slightly as θ increases to ~0.3 ML and then decreases as θ further increases, irrespective of the pump wavelength. Klünker *et al.*[31] studied on the coverage dependence of the K—Pt stretching mode on Pt(111) by high resolution electron energy loss spectroscopy (HREELS). The vibrational frequency shows blueshifts in the low coverage region (from 17 meV at 0.02 ML to 22 meV at ~0.16 ML) but shows redshifts when the coverage exceeds 0.2 ML (to 18.5 meV at 0.35 ML). While the blueshifts in the lower coverages are explained by dipole-dipole interaction among the adsorbates, the origin of the redshifts at higher coverages is not clear. The authors speculated that the redshifts are due to the K—Pt bond weakening in the higher coverage region or changes in adsorption sites. On the other hand, He and Jacobi[16] studied the Cs—Ru stretching mode on Ru(0001) by HREELS, and observed the similar coverage dependence of frequency as in the study of K/Pt(111).[31] The loss energy increases in the lower coverages (from 7 meV at 0.03 ML to 8.7 meV at 0.2 ML), while it decreases in $\theta>0.2$ ML (to 8.2 meV at 0.23 ML). They attributed the redshifts in higher coverages to the onset of metalization of the overlayer.

The coverage dependence of the Cs—Pt stretching frequency is similar to the alkali atoms on metal surfaces cited above. Here, we examine the frequency shift by dipole-dipole coupling. The vibrational frequency shift by dipole-dipole interaction depends on the coverage as[32]

$$\omega^2 = \omega_0^2 + \frac{q_0^{*}\Sigma_\theta}{M_r(1+\alpha_e\Sigma_\theta)}, \tag{4}$$

where ω_0 is the vibrational frequency at $\theta\rightarrow0$ ML, M_r is the reduced mass, q_0^* and α_e are the effective charge at the limit of zero coverage and the electronic polarizability of an adsorbate-substrate complex, respectively. We tried to fit the Cs—Pt frequencies observed in $0.18<\theta<0.35$ ML showing blueshifts with Eq. (4), but the number of data points is not sufficient to determine parameters in Eq. (4) uniquely. Then, we tentatively assume that the effective mass of metal atoms is so large that M_r is approximated by M_{Cs}. In this approximation only M_{Cs} is relevant to the stretching mode, thereby ω_0 for the Cs—Pt mode is fixed to that estimated for Cs/Ru(0001), i.e., 1.62 THz.[16] This enables us to determine the best fit parameter set, $q_0^*=0.32\pm0.03e_0$ and $\alpha_e=27\pm8$ $\mathrm{CV^{-1}\,m^2}$. The fitting result is depicted in Fig. 9(a). The effective charge is rather smaller than those estimated for K—Pt ($q_0^*=0.56e_0$) (Ref. 31) and Cs—Ru ($q_0^*=1.1e_0$).[16] This is because we neglect the bond weakening effects that also contribute in this coverage range where the fitting was made.

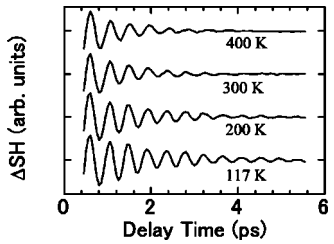

FIG. 11. Temperature dependence of the oscillatory TRSHG signals. Sample temperatures are indicated in the figure. The Cs coverage was 0.27 ML, and the absorbed fluence in 800-nm pump was 3.4 $\mathrm{mJ/cm^2}$.

H. Temperature dependence of oscillatory signals and the dephasing mechanism

Here we discuss the dephasing mechanism of the Cs—Pt stretching mode. Generally, the dephasing rate of vibrational coherence of adsorbate on a metal surface is given by

$$\Gamma = \gamma_{\mathrm{eh}} + \gamma_{\mathrm{ph}} + \gamma_{\mathrm{dep}}, \tag{5}$$

where γ_{eh} and γ_{ph} are dephasing rates by substrate electron-hole pair excitation and by direct coupling to substrate phonons, respectively, and γ_{dep} is a pure dephasing rate due to anharmonic coupling to other low frequency adsorbate-substrate modes or substrate phonon modes.

Figure 11 shows the oscillatory part of $\Delta\mathrm{SH}(t)$ obtained at various sample temperatures. These are the results obtained by using 800-nm pump at $\theta=0.27$ ML where the contribution of the Pt Rayleigh modes is negligible and the oscillatory signals are well represented by a single exponentially damped oscillation function. The frequency and the dephasing rate determined by a standard least- squares fitting with a single oscillation function are plotted in Fig. 12. As temperature increases, the frequency decreases, while the dephasing rate increases.

Graham *et al.*[33] observed systematic frequency shifts and line broadenings of frustrated translational modes of CO on Cu(001) as a function of temperature. These results were attributed to the growing hot bands of the translational modes whose frequencies are redshifted by the anharmonicity of the lateral CO—Cu potential curve. Alternatively, the anharmonic coupling between the nearly twofold degenerate

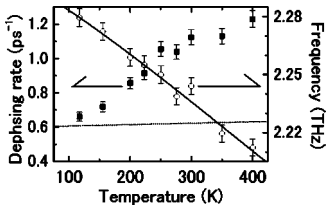

FIG. 12. Temperature dependence of the frequency (open circles) and dephasing rate (filled square) of the TRSHG oscillatory signals. Solid curve is a fitting of the frequency shift by Eq. (7). A dotted curve is the temperature dependence of the dephasing rate calculated from Eq. (8) with $\chi_e=0.0054$ and $\gamma_0=1.2$ ps^{-1}.

translational modes can cause the line shape variation observed.

We examine whether the variations in the central frequency and the dephasing rate plotted in Fig. 12 can also be interpreted by the hot bands as temperature increases. We adapt a Morse potential function along a Cs—Pt coordinate. The transition energy between the adjacent vibrational levels is given by

$$\Delta E_v = \hbar\omega_0[1 - 2\chi_e(v+4)], \tag{6}$$

where χ_e is an anharmonic coupling parameter and v is a vibrational quantum number. As temperature increases, the transitions from higher vibrational states contribute to the spectra, resulting in a mean transition energy,

$$\Delta E(T) = \frac{\Sigma_v \Delta E_v e^{-E(v)/kT}}{\Sigma_v e^{-E(v)/kT}}. \tag{7}$$

As for the incoherent frequency domain spectroscopy (i.e., He-atom scattering), the total linewidth, Γ_w, including the contribution of hot bands is given by

$$\Gamma_w = \sqrt{\frac{\Sigma_v[\Delta E_v - \Delta E(T)]^2 e^{-E(v)/kT}}{\Sigma_v e^{-E(v)/kT}}} + \gamma_0, \tag{8}$$

where γ_0 is the temperature independent width. Here, we assume that all the contributions of the vibrational coherence with the higher vibrational quantum numbers overlap in-phase in TRSHG signals, and that the vibrational dephasing rate is independent of v. Then, the dephasing rate Γ is related to Γ_w as $\Gamma=\Gamma_w/2$. In Fig. 12, the observed peak shifts are well reproduced by Eq. (7) with an anharmonicity parameter of $\chi_e=0.0054\pm0.0006$ and $\omega_0=2.32\pm0.01$ THz. In contrast, the dephasing rate cannot be reproduced by Eq. (8) with the same χ_e. Thus, the temperature dependence of dephasing rates cannot be interpreted by the simple model that takes into account only the anharmonic shift in the Cs—Pt vibrational frequency.

The frequencies of parallel (longitudinal) modes in a Cs adlayer on Cu(001) were found in 0–5 meV (0–1.2 THz) by helium atom scattering.[17] The parallel modes of Cs/Pt(111) system likely fall in the similar frequency range. Since the frequencies are very low, they are populated thermally at the temperatures used in the current study. Thus, the anharmonic coupling between the Cs—Pt stretching mode and the parallel modes enhances the dephasing rate as temperature increases. This pure dephasing is likely to be the dominant mechanism for the temperature dependence of dephasing rates.

Now we discuss which damping term in Eq. (5) dominates over the others. Since the frequency of the Cs—Pt stretching mode is below the maximum phonon frequency of bulk Pt, the contribution of $\gamma_{\rm ph}$ to the total damping rate would be large. The friction parameter $\eta_\perp$ for the damping of a perpendicular mode via direct coupling to the substrate can be estimated by using the elastic continuum model by Persson as,[34]

$$\eta_\perp = \frac{m\omega^2 n_a}{\rho_d c_L}, \tag{9}$$

where m is adsorbate mass, ρ_d is the density of substrate, c_L is the longitudinal sound velocity of substrate, n_a is the number density of the adsorbate, and ω is the oscillation frequency. Introducing $m=133$ u, $\omega=76$ cm^{-1}, and $n_a=0.27$ ML in Eq. (9), we estimate $\gamma_{\rm ph}=\eta_\perp/2$ to be ~1.0 ps^{-1}. This is close to the experimental results.

However, the reduction of the dephasing time is more significant. The dephasing time of the Cs—Pt stretching mode decreases by more than 50% as the coverage increases up to $\theta=0.38$ ML, i.e., from $1/\Gamma>1.0$ ps at $0.24<\theta<0.32$ ML to $1/\Gamma=0.5$ ps at $\theta=0.38$ ML. According to Eq. (9), $\gamma_{\rm ph}$ increases linearly to the coverage. Thus, this theory predicts that the dephasing time at $\theta=0.38$ ML to be $\sim63\%$ of that at $\theta=0.24$ ML. The further reduction in τ would be due to the increased disorder of the overlayer structure and/or due to the enhancement of the anharmonic coupling with the parallel modes.

When the first layer of Cs is completed, the dephasing time is elongated to more than 1.5 ps, indicating that the linear relation predicted by Eq. (9) between the dephasing time and the coverage is no longer valid. It has been pointed out that in an incommensurate layer $\gamma_{\rm ph}$ could be substantially small due to the destructive interference of emitted substrate phonons with long wavelengths.[34] This mechanism well explains the sudden change of the dephasing time at $\theta\sim0.41$ ML.

On the other hand, there would be a substantial contribution of $\gamma_{\rm eh}$ to the total dephasing rate, since Cs strongly chemisorbs on Pt(111). The amount of $\gamma_{\rm eh}$ is represented by the charge fluctuation δn during the vibrational period as,[35]

$$\gamma_{\rm eh} = \pi\omega(\delta n)^2. \tag{10}$$

Without knowing the amount of δn, it is impossible to estimate the magnitude of $\gamma_{\rm eh}$. Thus, we estimate the upper limit of δn from the total dephasing rate observed; $\gamma_{\rm eh}<1$ ps^{-1} at $\theta=0.27$ ML results in $\delta n<0.37$.

IV. SUMMARY

We have investigated how the nuclear wavepacket motion of Cs adsorbed on Pt(111) depends on Cs coverage and surface temperature by femtosecond time-resolved second harmonic generation. The oscillatory components in TRSHG signals are attributed to the vibrational coherence at the surface. The most prominent component is the one in 2.2–2.4 THz caused by the nuclear wavepacket dynamics of

Cs—Pt stretching in the ground state. For 580-nm pump, the wavepacket motion of the Cs—Pt stretching mode appears at $\theta > 0.18$ ML and its coherent amplitude has a sharp maximum in $\theta \sim 0.36$ ML. On the other hand, the wavepacket motion is observed in $0.26 < \theta < 0.38$ ML with a broad maximum for 800-nm pump. These features indicate that the vibrational coherence is enhanced by the electronic resonant excitation between Cs derived surface states in the coverage range.

The LPSVD analysis revealed that the additional components with frequency higher than 2.45 THz are contained in the oscillatory signals. The frequencies of the additional components are 2.5–2.6 THz in $0.22 < \theta < 0.29$ ML, and ~2.9 THz in $0.29 < \theta < 0.37$ ML. These components are assigned to the Rayleigh phonon modes of the Pt substrate. In $\theta > 0.39$ ML, the other component with frequency of ~2.5 THz gains a large amplitude for 580-nm pump, whose origin is not clear at this stage.

The frequency of the Cs—Pt stretching mode shows blueshifts in $0.18 < \theta < 0.35$ ML but redshifts in $0.35 \leqslant \theta \leqslant 0.41$ ML as Cs coverage is increased. This frequency shifts are determined to the balance between the dipole-dipole coupling among the adsorbates and bond weakening associated with structural changes. The dephasing time of the Cs—Pt mode becomes shorter as the coverage increases until the first layer is completed. This is attributed to the adlayer structural change and/or the enhancement in the damping rate by one-phonon emission to the substrate. The temperature dependence of the dephasing dynamics and the oscillation frequency of the Cs—Pt mode could not be interpreted simply by contributions of hot bands. Instead, they are possibly due to pure dephasing by anharmonic coupling between the Cs—Pt stretching and parallel modes.

ACKNOWLEDGMENTS

This work was supported in part by Grants-in-Aid for Young Scientists (A)(14703009), Scientific Research on Priority Area (417), Creative Scientific Research Collaboratory on Electron Correlation-Toward a New Research Network between Physics and Chemistry (13NP0201) from the Ministry of Education, Culture, Sports, Science and Technology (MEXT) of Japan, and KAKENHI (14340176) from Japan Society for the Promotion of Science (JSPS).

*Electronic address: matsumoto@ims.ac.jp

[1] Y. M. Chang, L. Xu, and W. K. Tom, Phys. Rev. Lett. **78**, 4649 (1997).
[2] Y. M. Chang, L. Xu, and W. K. Tom, Chem. Phys. **251**, 283 (2000).
[3] K. Watanabe, N. Takagi, and Y. Matsumoto, Phys. Rev. B **65**, 235328 (2002).
[4] K. Watanabe, N. Takagi, and Y. Matsumoto, Chem. Phys. Lett. **366**, 606 (2002).
[5] K. Watanabe, N. Takagi, and Y. Matsumoto, Phys. Rev. Lett. **92**, 057401 (2004).
[6] D. Ino, K. Watanabe, N. Takagi, and Y. Matsumoto, Chem. Phys. Lett. **383**, 261 (2004).
[7] H. W. K. Tom, C. M. Mate, X. D. Zhu, J. E. Crowell, T. F. Heinz, G. A. Somorjai, and Y. R. Shen, Phys. Rev. Lett. **52**, 348 (1984).
[8] H. W. K. Tom, C. M. Mate, X. D. Zhu, J. E. Crowell, Y. R. Shen, and G. A. Somorjai, Surf. Sci. **172**, 466 (1986).
[9] S. A. Lindgren and L. Walldén, Phys. Rev. B **45**, 6345 (1992).
[10] S. Reiff, W. Drachsel, and J. H. Block, Surf. Sci. Lett. **304**, L420 (1994).
[11] B. N. J. Persson and L. H. Dubois, Phys. Rev. B **39**, 8220 (1989).
[12] A. Liebsch, Phys. Rev. B **40**, 3421 (1989).
[13] N. Fischer, S. Schuppler, T. Fauster, and W. Steinmann, Surf. Sci. **314**, 89 (1994).
[14] G. Hoffmann, J. Kliewer, and R. Berndt, Phys. Rev. Lett. **87**, 176803 (2001).
[15] T. A. Germer, J. C. Stephenson, E. J. Heilweil, and R. R. Cavanagh, J. Chem. Phys. **98**, 9986 (1993).
[16] P. He and K. Jacobi, Phys. Rev. B **53**, 3658 (1996).
[17] G. Witte and J. P. Toennies, Phys. Rev. B **62**, R7771 (2000).
[18] S. Mukamel, *Principles of Nonlinear Optical Spectroscopy* (Oxford, New York, 1995), Chap. 6.
[19] W. T. Pollard, H. L. Fragnito, J. Y. Bigot, C. V. Shank, and R. A. Mathies, Chem. Phys. Lett. **168**, 239 (1990).
[20] J. Chesnoy and A. Mokhtari, Phys. Rev. A **38**, 3566 (1988).
[21] R. Scholz, M. Schreiber, F. Bassani, M. Nisoli, S. D. Silvestri, and O. Svelto, Phys. Rev. B **56**, 1179 (1997).
[22] S. L. Dexheimer, A. D. V. Pelt, J. A. Brozik, and B. I. Swanson, Phys. Rev. Lett. **84**, 4425 (2000).
[23] Y. Kayanuma and S. Tanaka, Phys. Rev. B **62**, 12 838 (2000).
[24] H. Petek, M. J. Weida, H. Nagano, and S. Ogawa, Science **288**, 1402 (2000).
[25] H. Barkhuijsen, R. D. Beer, W. M. M. J. Bovée, and D. van Ormondt, J. Magn. Reson. (1969-1992) **61**, 465 (1985).
[26] A. E. Johnson and A. B. Myers, J. Chem. Phys. **104**, 2497 (1996).
[27] J. Cousty and R. Riwan, Surf. Sci. **204**, 45 (1988).
[28] T. Kondo, H. Kozakai, T. Sasaki, and S. Yamamoto, J. Vac. Sci. Technol. A **19**, 2866 (2001).
[29] U. Harten, J. P. Toennies, C. Wöll, and G. Zhang, Phys. Rev. Lett. **55**, 2308 (1985).
[30] G. A. Garrett, T. F. Albrecht, J. F. Whitaker, and R. Merlin, Phys. Rev. Lett. **77**, 3661 (1996).
[31] C. Klünker, C. Steimer, J. B. Hannon, M. Giesen, and H. Ibach, Surf. Sci. **420**, 25 (1999).
[32] H. Ibach and D. L. Mills, *Energy Loss Spectroscopy and Surface Vibrations* (Academic, New York, 1982).
[33] A. Graham, F. Hofmann, and J. P. Toennies, J. Chem. Phys. **104**, 5311 (1996).
[34] B. N. J. Persson, E. Tosatti, D. Fuhrmann, G. Witte, and C. Wöll, Phys. Rev. B **59**, 11 777 (1999).
[35] B. N. J. Persson and M. Persson, Solid State Commun. **36**, 175 (1980).